JBC RESEARCH ARTICLE

Downregulation of PIK3IP1/TrIP on T cells is controlled by TCR signal strength, PKC, and metalloprotease-mediated cleavage

Received for publication, April 4, 2024, and in revised form, October 15, 2024 Published, Papers in Press, October 24, 2024,
https://doi.org/10.1016/j.jbc.2024.107930

Benjamin M. Murter[1,2], **Sean C. Robinson**[1], **Hridesh Banerjee**[1], **Louis Lau**[1,2], **Uzodinma N. Uche**[1], **Andrea L. Szymczak-Workman**[1], **and Lawrence P. Kane**[1,*]

From the [1]*Department of Immunology, and* [2]*Graduate Program in Microbiology and Immunology, University of Pittsburgh, Pittsburgh, Pennsylvania, USA*

Reviewed by members of the JBC Editorial Board. Edited by Philip A. Cole

The protein known as PI3K-interacting protein (PIK3IP1), or transmembrane inhibitor of PI3K (TrIP), is highly expressed by T cells and can modulate PI3K activity in these cells. Several studies have also revealed that TrIP is rapidly downregulated following T cell activation. However, it is unclear how this downregulation is controlled. Using a novel monoclonal antibody that robustly stains cell-surface TrIP, we demonstrate that TrIP is lost from the surface of activated T cells in a manner dependent on the strength of signaling through the T cell receptor and specific downstream signaling pathways, in particular classical PKC isoforms. TrIP expression returns by 24 h after stimulation, suggesting that it may play a role in resetting T cell receptor signaling at later time points. We also provide evidence that ADAM family proteases are required for both constitutive and stimulation-induced downregulation of TrIP in T cells. Finally, by expressing truncated forms of TrIP in cells, we identify the region in the extracellular stalk domain of TrIP that is targeted for proteolytic cleavage.

Signaling pathways controlled by phosphoinositide (PI) intermediates are ubiquitous regulators of cell growth, survival, and transformation (1). Key signal transducers in this pathway include various phosphatidylinositol 3-kinases (PI3K), which catalyze phosphorylation of PI species at the 3′ position of the inositol ring to produce PIP_3 and related species. The second messenger PIP_3 acts to recruit pleckstrin homology domain-containing proteins like Akt to the plasma membrane. In total, four different catalytic subunits (α, β, γ, and δ) comprise the PI3K family, which pair with adaptor subunits that allosterically regulate PI3K activation (2–4). The major PI3K isoform linked to T cell activation is PI3Kδ. The PI3K signaling pathway is a significant mediator of activation, survival, and differentiation signals downstream of the T cell receptor (TCR) and CD28, integrating antigen recognition and costimulatory signals, respectively (5–8). Additionally, interleukin 2 (IL-2) and IL-15 cytokine receptors also activate PI3Ks to modulate T cell survival and function (9). Counter-regulating these activating signals are several phosphatases, most notably the lipid-phosphatase and tumor suppressor PTEN, which regulate these signals and tune the T cell response (10). *In vivo*, dysregulation of PI3K signaling in T cells can lead to the development of hematological malignancy or immunodeficiency (11–13).

While it has long been known that PI3Ks are activated in response to TCR for antigen and costimulatory molecule (*e.g.* CD28) engagement, the precise role of this pathway in T cell responses has been more challenging to parse. Andreotti *et al.* previously demonstrated that the PI3K signaling pathway plays a more nuanced role in T cell biology (14) when compared with the critical TCR-proximal kinases (Lck and Zap70) and adaptor proteins (LAT and SLP-76). Thus, a fuller understanding of the role of this pathway in T cell biology has required *in vivo* approaches, where more subtle mechanisms can be revealed through downstream effects on T cell differentiation.

We and others recently reported that T cell activation can be modulated by a novel negative regulator of PI3K that we have referred to as transmembrane inhibitor of PI3K (transmembrane inhibitor of PI3K (TrIP); gene name *PIK3IP1*) (15–17). Unique among known negative regulators of PI3Ks, TrIP is a transmembrane protein that contains an SH2-homology domain toward its C terminus similar to the inter-SH2 domain of p85α/β, which are critical upstream positive regulators of PI3K catalytic subunit (p110 family) activation. Although the precise molecular mechanism by which TrIP functions is not clear, evidence suggests that TrIP specifically interacts with p85 that is recruited to phospho-Tyr residues in proteins like CD28, which in turn interferes allosterically with the activation of p110 by p85. This interaction between TrIP and the p110/p85 heterodimer has been shown to negatively regulate the catalytic activity of PI3K and inhibit downstream signaling (18).

Although initial studies on TrIP shed light on its roles in T cell activation, they were somewhat limited by the lack of a suitable monoclonal antibody (mAb) that could assay cell-surface expression of TrIP. In this study, we detail the production and validation of such antibodies, focusing on the

* For correspondence: Lawrence P. Kane, lkane@pitt.edu.

highest sensitivity mAb clone 18E10. We have used this antibody to characterize the levels of TrIP on various immune cell types, finding that neutrophils and $CD8^+$ T cells have particularly high expression. We confirm that endogenous cell-surface TrIP protein is lost upon TCR activation of $CD8^+$ T cells, and that this downregulation is related to the strength of activating TCR signal. We also are the first to report that although highly expressed on naïve cells, TrIP expression on $CD8^+$ T cells does return at later time points following activation. Additionally, we have found that protein kinase C (PKC) activation downstream of TCR signaling is required to trigger the downregulation of TrIP surface expression. Furthermore, we have determined that matrix metalloproteases of the ADAM family are responsible for the downregulation of endogenous TrIP protein from activated T cells. Finally, we found that TrIP downregulation is mediated by site-specific cleavage in the stalk domain. Taken together, these studies advance our knowledge of both how TrIP is regulated at the cellular level, and how this is tied to initiation of T cell activation. Our identification of a noncleavable form of TrIP should promote further understanding of the wider biological effects of this protein *in vivo*.

Results

Development of monoclonal antibodies to murine TrIP

The *in vivo* study of TrIP function has been hampered by the lack of suitable antibodies, especially against the extracellular domain of the protein. We therefore generated an Ig fusion protein by cloning the extracellular domain of TrIP into a vector encoding the Fc region from human IgG1 (TrIP-Ig; Fig. 1*A*). This construct was then used to produce recombinant TrIP-Ig by transfection into HEK293T cells. After confirming its integrity by SDS-PAGE (Fig. 1*B*), TrIP-Ig was used to immunize rats. Spleens of immunized rats were harvested and fused with myeloma cells to generate hybridomas. Supernatants from stable clones were then screened against TrIP-Ig and counter-screened against human IgG1. Supernatants from three sub-clones were then screened for the ability to recognize murine TrIP (mTrIP) by flow cytometry. Initially, HEK293T cells were transiently transfected with a Flag-tagged mTrIP (Flag-mTrIP) construct and labeled with supernatant from each anti-TrIP mAb clones. Following up with an anti-rat IgG secondary to label the clones with a fluorophore we show in Figure 1*C*, all three of these mAb's specifically bound to cells expressing Flag-mTrIP, showing double positive staining for Flag as control. The degree of binding, however, varied by clone with 18E10 showing the most robust labeling of mTrIP based on colabeling with an anti-Flag mAb (Fig. 1*C*). We also screened the anti-TrIP clones for cross-reactivity with human TrIP, as mouse and human TrIP are approximately 80% identical, and therefore could potentially cross-react (18). Although not seen with all three mAb's, the 18E10 clone displayed significant cross-reactivity with ectopically expressed human TrIP (Fig. 1*D*). We next determined which of the two major extracellular regions, the stalk domain or the kringle domain, the novel anti-TrIP mAb's were binding. To test this, we compared binding of the Ab's to full-length TrIP *versus* a construct engineered to lack the kringle domain, but still bearing an N-terminal Flag-tag on the stalk for detection. Despite robust Flag staining, binding of all the mAb's was lost in the absence of the kringle domain (mTrIP-ΔKringle) (Fig. 1*E*). These data demonstrate the successful generation of several monoclonal anti-murine TrIP antibody clones, which bind *via* its kringle domain. Additionally, we found that the most sensitive mAb (18E10) shows cross-reactivity against human TrIP.

Expression of TrIP on normal murine splenocytes

We next wanted to confirm that the newly generated anti-mTrIP mAb could recognize endogenous levels of protein. Thus, we directly conjugated anti-mTrIP mAb 18E10 to Alexa Fluor 647 for use in multicolor flow cytometry. Previous reports (17, 19, 20) and public data sets (21) show that TrIP expression is not only restricted to the T cell compartment. Therefore, we incorporated the 18E10 mAb in a large spectral flow cytometry panel for murine splenocytes to assess TrIP expression more broadly. Using the ExCYT software package (https://github.com/sidhomj/ExCYT) (22), we performed high-dimensional clustering analysis (t-SNE) of these data and were able to identify a wide range of cell types (Fig. 2*A*). Next, we overlayed the expression pattern of TrIP as a heatmap (Fig. 2*B*), which revealed expression across cell types, with especially robust expression on $CD8^+$ T cells ($CD3^+CD8^+$), whereas Treg ($CD3^+CD4^+Foxp3^+$) and conventional CD4 ($CD3^+CD4^+Foxp3^-$) had much lower expression in comparison (Fig. 2, *C* and *D*). Of the major myeloid populations characterized, we did find moderate levels of TrIP expression on macrophages ($CD11b^+F4/80^+$), and the highest levels of TrIP expression were seen in the neutrophils ($CD11b^+Gr1^{Hi}$) (Fig. 2, *C* and *D*). In parallel, we also labeled splenocytes from a CD8-specific TrIP KO mouse ($TrIP^{fl/fl}$ x $E8i^{Cre}$), a mouse model previously generated in our lab, as a negative control (16). Thus, the 18E10 mAb robustly stained WT $CD8^+$ T cells from naïve C57BL/6 mice, but not those from CD8-specific TrIP KO mice (Fig. 2*E*) confirming the staining specificity and sensitivity to endogenous levels of the protein.

Previous work from our lab and others has suggested that TrIP expression is high on resting cells but is downregulated upon T cell activation (15–17). In support of these data, staining of endogenous TrIP revealed that over 90% of splenic $CD8^+$ T cells are $TrIP^+$ (Fig. 2, *E* and *H*). Furthermore, subsetting these cells based on their activation status revealed that TrIP was indeed expressed at much lower levels on effector ($CD44^+$), *versus* naïve/resting ($CD62L^+$) T cells (Fig. 2, *F* and *G*). Our previous studies using cell line expression of epitope-tagged TrIP suggested that TrIP surface expression is lost upon activation (16), so we wanted to confirm that endogenous TrIP protein behaves in a similar manner. To test this, we subjected WT P14 splenocytes to plate-bound anti-CD3/anti-CD28 stimulation, and followed the expression of TrIP with the 18E10-AF647 mAb out to 24 h after stimulation. As shown in Figure 2, *H* and *I*, TrIP surface expression was rapidly lost

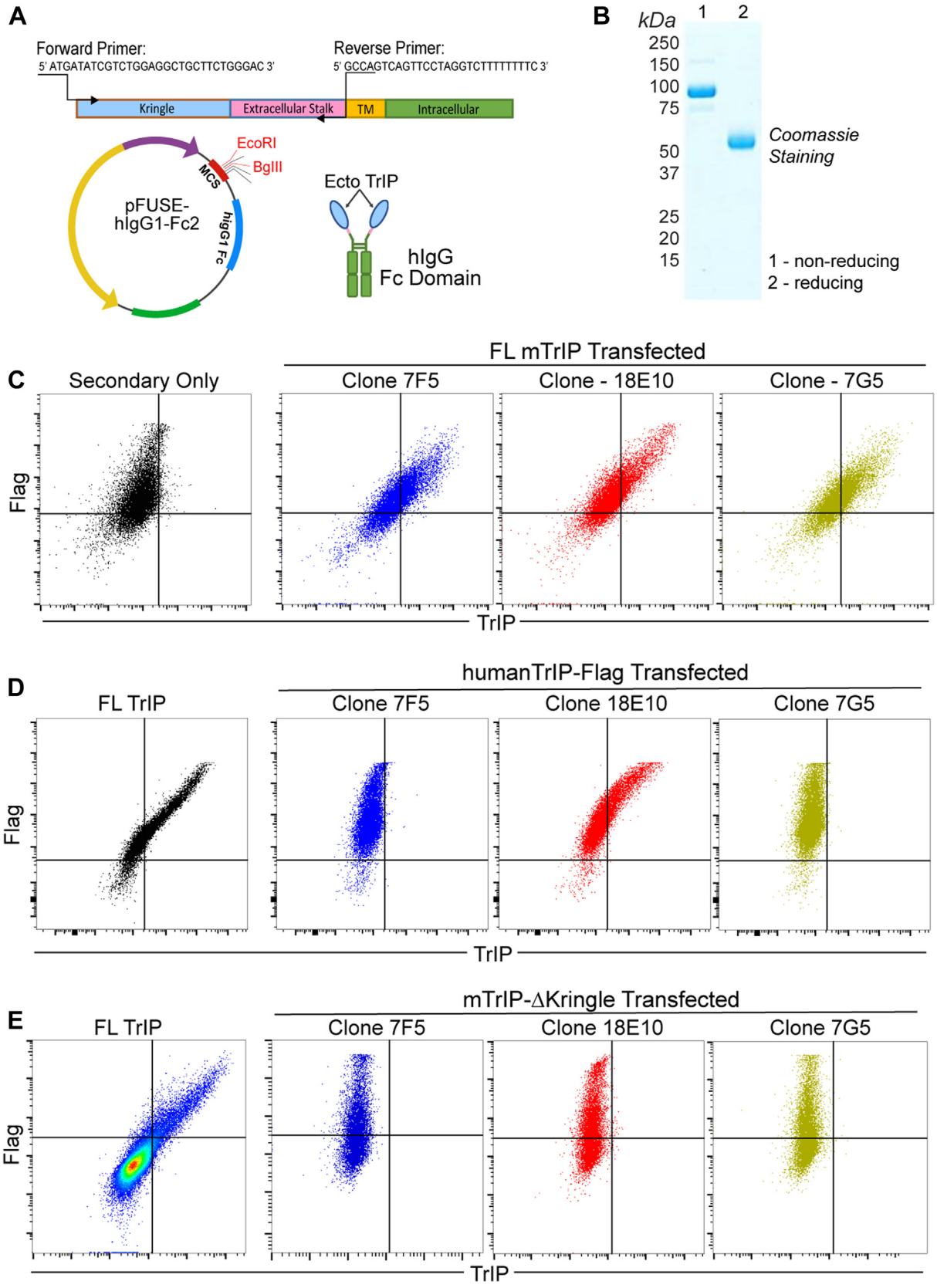

Figure 1. Development and validation of novel monoclonal antibodies to the ecto domain of TrIP. *A*, cloning strategy and development of the ecto-TrIP Fc-fusion protein used for immunization and antibody development. *B*, SDS-PAGE of the ectoTrIP-Ig fusion protein under reducing and nonreducing conditions. *C*, flow cytometry data showing the binding of each anti-TrIP monoclonal antibody to a Flag-tagged WT murine TrIP construct expressed in HEK293T cells. *D*, flow cytometry data showing staining of the clones on HEK293T cells transfected with a plasmid encoding Flag-tagged human TrIP. *E*, flow cytometry data showing the staining of each of the anti-TrIP mAbs on HEK293T cells transfected with a Flag-tagged mTrIP construct lacking the extracellular kringle domain (ΔKringle). HEK, human embryonic kidney; mAb, monoclonal antibody; mTrIP, murine TrIP; TrIP, transmembrane inhibitor of PI3K.

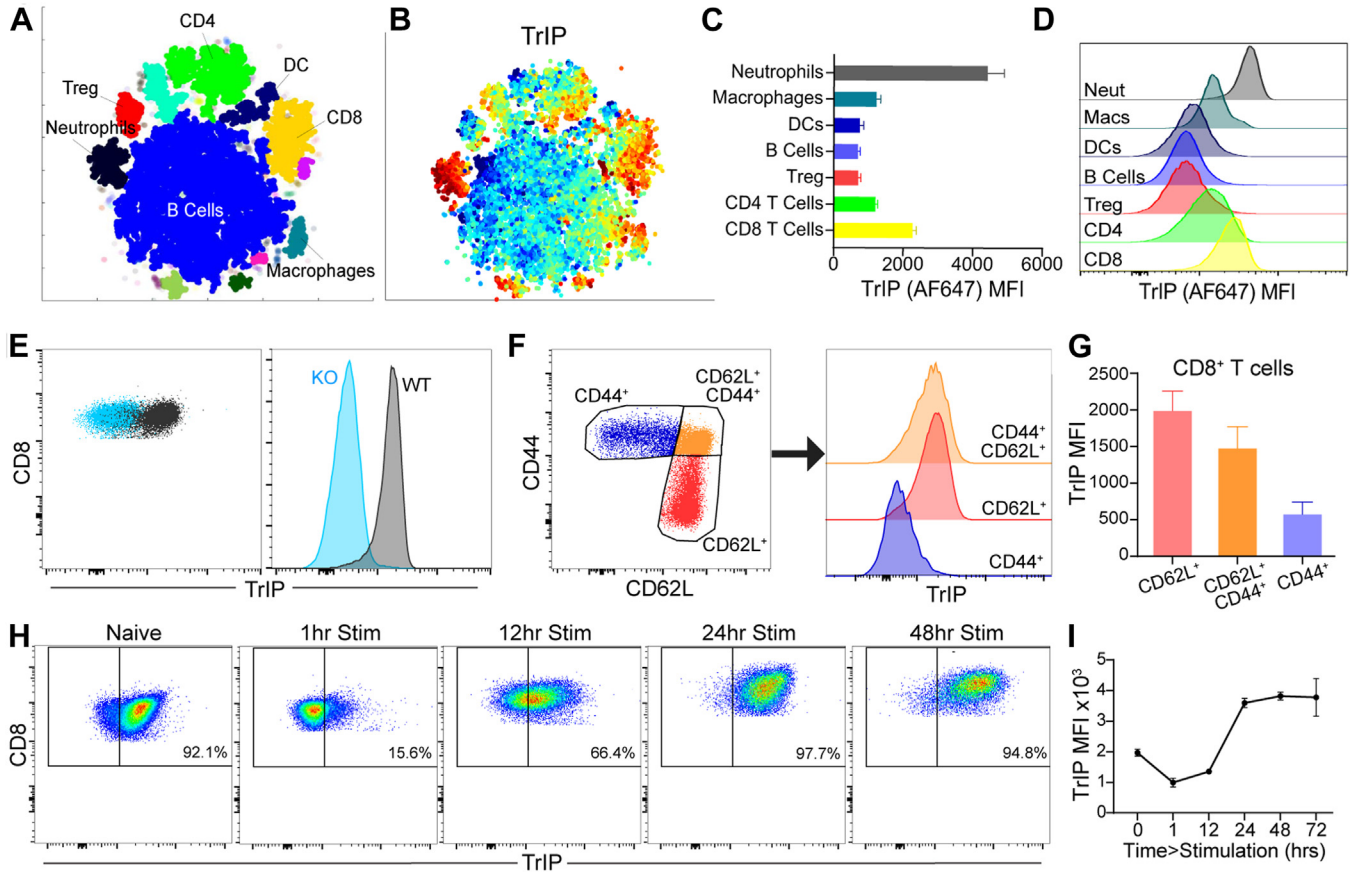

Figure 2. Characterization of TrIP expression on immune cells in naïve mice. *A*, ExCYT clustering analysis of flow cytometry data identifies major splenic populations including B cells ($CD19^+$), CD4 ($CD3^+CD4^+FoxP3^-$) and CD8 ($CD3^+CD8^+$) T cells, regulatory T cells ($CD3^+CD4^+FoxP3^+$), DCs ($CD11c^+$), macrophages ($CD11b^+F4/80^+$), and neutrophils ($CD11b^+Gr\text{-}1^{Hi}$) (22). *B*, heatmap of TrIP protein expression overlayed across the splenic populations. *C*, quantification of TrIP expression by MFI across each of the immune cell populations. *D*, histograms depicting the range of TrIP expression in the indicated populations. *E*, staining of WT *versus* TrIP KO (*Pik3ip1*$^{fl/fl}$*E8i*^{cre}) $CD8^+$ T cells ($CD3^+CD8^+$) from naïve spleens as a dot plot and histogram. *F*, gating strategy for naïve ($CD62L^+$) and activated ($CD44^+$) $CD8^+$ T cells and corresponding histograms of their TrIP expression. *G*, quantification of TrIP MFI in the $CD8^+$ T cell subpopulations, stratified by their CD44 versus CD62L expression. *H*, stimulation of whole WT P14 TCR Tg splenocytes with 200 ng/ml of WT gp33 peptide. TrIP was followed over 72 h by flow cytometry. *I*, quantification of TrIP expression MFI on $CD8^+$ T cells in the 72 h following activation *in vitro*. MFI, mean fluorescence intensity; PIK3IP1, PI3K-interacting protein; TCR, T-cell receptor; TrIP, transmembrane inhibitor of PI3K.

within the first 2 h of stimulation and remained at very low levels for about 12 h. To date, it has been unclear when, or even if, TrIP expression reoccurs following T cell activation. As shown in Figure 2, *H* and *I*, we found that $CD8^+$ T cells begin to reexpress TrIP around 12 h following activation and fully reexpress TrIP by 24-48 h.

Kinetics of TrIP downregulation on activated T cells correlates with TCR signal strength

Existing data suggest that TrIP acts as a "rheostat" for initial PI3K and T cell activation downstream of the TCR. Therefore, we wanted to assess the relationship of TCR signal strength to the putative cleavage of TrIP after activation. Using 18E10-AF647 mAb to assay TrIP levels over time, we stimulated splenocytes from WT C57BL/6 mice with varying concentrations of plate-coated anti-CD3 plus anti-CD28 mAb's. We found that the kinetics of TrIP loss correlated with the strength of stimulation, in a roughly semilogarithmic fashion (Fig. 3, *A* and *B*). Next, we tested the relative contributions of signal 1 (TCR/CD3) and signal 2 (CD28 co-stimulation) on the downregulation of TrIP following activation. To block CD28 costimulation, we pretreated WT splenocytes with saturating amounts of CTLA4-Ig prior to stimulation with anti-CD3 mAb. These experiments suggested that the loss of TrIP does not require CD28 costimulation, as the degree and timing of TrIP downregulation were nearly identical with or without CD28 blockade (Fig. 3, *C* and *D*).

To assess the sensitivity of TrIP loss to changes in TCR signal strength under more physiological conditions, we performed stimulation of T cells with antigen and antigen-presenting cells. We thus stimulated splenocytes from P14 TCR Tg mice with cognate antigen (LCMV gp33 peptide presented by H-$2D^b$) and measured levels of cell surface TrIP on $CD8^+$ P14 T cells over time, by flow cytometry. As shown in Figure 3*E*, we observed rapid and dramatic loss of cell-surface TrIP upon stimulation with gp33 peptide, similar to what we had observed after stimulation with anti-CD3 mAb. Importantly, this system also allowed us to test the effects of altered gp33 peptides with different affinities for the P14 TCR (23). Shown in Figure 3, *E* and *F* are the results with two such peptides, with the higher affinity peptide (HiAff gp33)

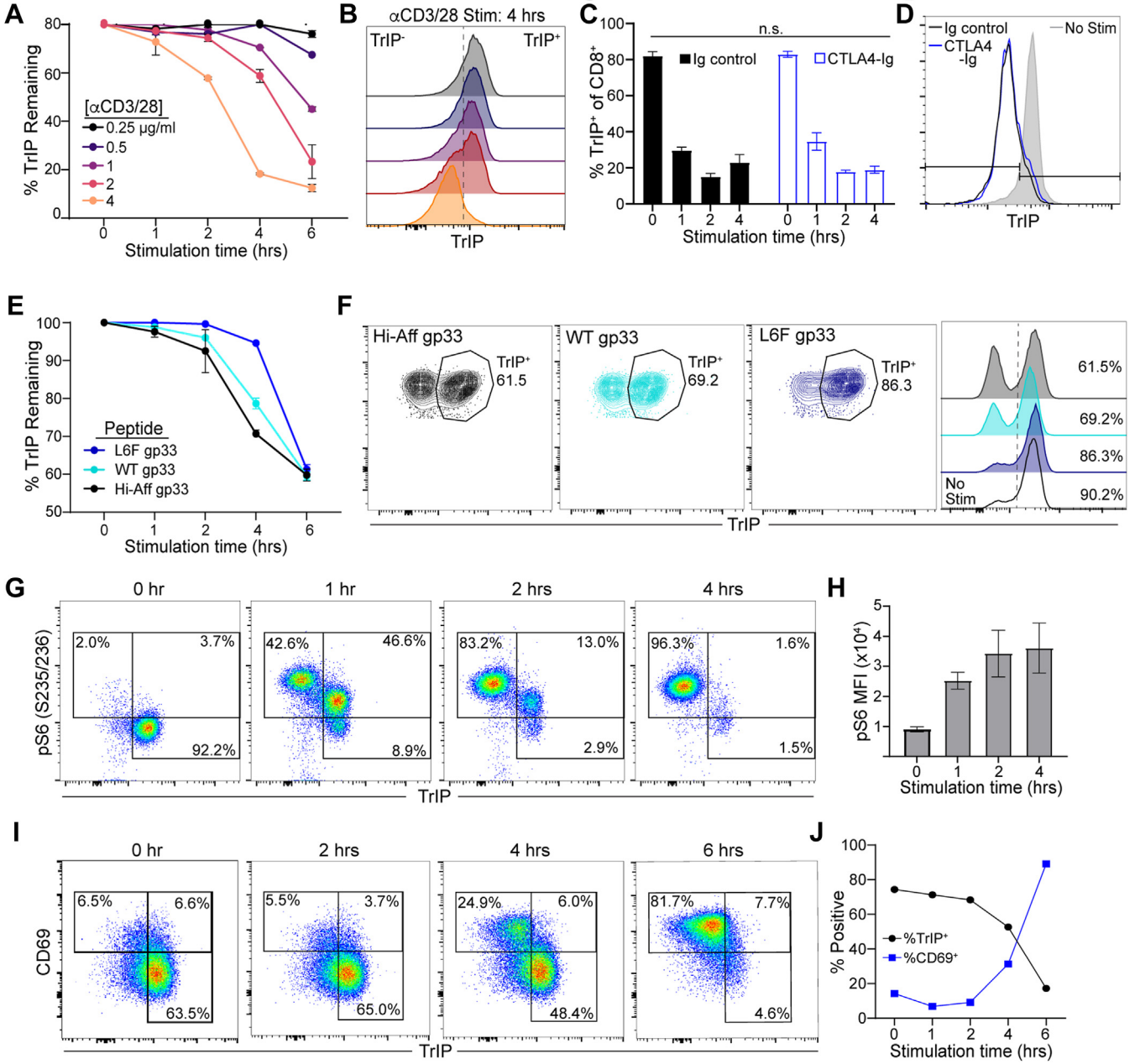

Figure 3. Stimulation strength-dependent downregulation of TrIP on CD8$^+$ T cells. *A*, WT C57BL/6 splenocytes were stimulated with plate-coated anti-CD3 and anti-CD28 at the indicated concentrations and TrIP loss on the CD8$^+$ T cells was followed over time by flow cytometry. *B*, histogram of the TrIP expression on CD8$^+$ T cells at the 4-h time point of each stimulation dose. *C*, WT B6 splenocytes stimulated with 2 μg/ml of plate-coated anti-CD3 in the presence or absence of saturating amounts of CTLA4-Ig (20 μg/ml). *D*, representative histogram overlay of CTLA4ig blockade experiment at the 1-h time point. *E*, WT P14 TCR Tg splenocytes were stimulated with 100 ng/ml of the indicated cognate peptide variants (peptide affinity: Hi-Aff gp33>WT gp33 > L6F gp33) and followed TrIP expression on the CD8$^+$ T cells over time *via* flow cytometry. *F*, representative TrIP staining of each peptide stimulation at the 4-h time point, shown by both dot plot and histogram overlays. *G*, WT P14 splenocytes stimulated with 200 ng/ml of WT gp33 peptide showing staining for pS6$_{(S235/S236)}$ *versus* TrIP staining in the CD8$^+$ T cells following activation. *H*, quantification of pS6$_{(S235/S236)}$ MFI during the 4-h course of stimulation. *I*, in the same WT P14 stimulation described in *G* and *H*, flow plots depicting CD69 *versus* TrIP expression through 6 h of stimulation. *J*, frequencies of total TrIP$^+$ and total CD69$^+$ cells. Ordinary two-way ANOVA used for statistical comparisons (*p*: *<0.05, **<0.01, ***<0.001, ****<0.0001). MFI, mean fluorescence intensity; pS6, phosphorylation of the S6 ribosomal subunit; TCR, T-cell receptor; TrIP, transmembrane inhibitor of PI3K.

triggering the greatest degree of TrIP downregulation (>30%) by 4 h after stimulation. By contrast, a lower affinity peptide (L6F gp33) caused very little TrIP loss after 4 h (<5%). Thus, these data demonstrate that peptide/MHC affinity for the TCR is tightly linked with the kinetics of TrIP downregulation.

Although the functional relevance of acute cell-surface TrIP downregulation is not completely clear, such down-modulation of a negative regulator like TrIP may help to constrain early T cell activation, as suggested in previous publications from our group and others (16, 17). Consistent with this notion, we found that WT P14 CD8 T cells activated with cognate peptide seem to progress through three distinct stages of early T cell activation, distinguished by their relative expression of TrIP and phosphorylation of the S6 ribosomal

subunit (pS6) (Fig. 3*G*). Starting with a naïve (*i.e.* TrIP$^+$) population of CD8$^+$ T cells, we found that after 1 h of stimulation with 200 ng/ml of WT gp33 peptide, a small proportion (<10%) of the cells had yet to undergo activation, indicated by a lack of pS6 staining. Somewhat unexpectedly, we found a distinct population of pS6-intermediate (pS6^{int}) cells which still maintained TrIP expression. This intermediate pS6 intensity is consistent with the regulatory activity that TrIP plays during early T cell activation, as loss of TrIP coincides with a secondary increase in pS6 signal intensity that then persists beyond 4 h of stimulation (Fig. 3*H*). These data further suggest that the loss of TrIP is not a prerequisite for active PI3K signaling, but rather may act to modulate PI3K signal intensity at the early stages of CD8$^+$ T cell activation. To provide additional functional context to TrIP expression following T cell activation, we assessed whether there was a temporal association between TrIP downregulation and expression of a well-established early indicator of T cell activation, CD69. As shown in Figure 3*I*, we did in fact observe a tightly associated inverse correlation between loss of cell-surface TrIP and expression of CD69 (Fig. 3*J*).

Role of TCR-dependent signaling pathways in acute downregulation of TrIP

Next, we sought to understand which TCR signaling pathways regulate the stimulation-induced turnover of TrIP surface expression. Initially, we hypothesized that the pS6 upregulation that occurs while still maintaining TrIP expression that we saw previously (Fig. 3*G*) may be a prerequisite for TrIP loss. This idea suggests that PI3K signaling itself may act in a feed-forward loop, directly leading to TrIP downregulation. To investigate this, we took a pharmacological approach, using well-defined inhibitors to target various PI3K pathway members, including PI3K itself (IC87114), Akt (MK2206), and mTORC1 (rapamycin). Using WT P14/cognate gp33 peptide stimulation, we pretreated with the indicated inhibitors for 30 min prior to the addition of a 200 ng/ml dose of WT gp33 peptide. We found that treatment with each of these inhibitors resulted in a modest (∼10%) higher expression of TrIP up to 2 h after stimulation, compared to the control (Fig. 4, *A* and *B*). While these inhibitors did modestly slow the loss of TrIP, they did not seem to impact baseline expression levels, despite drug exposure for the entire assay ("0 h" samples) nor do they lead to persistence at later time points (4 h time points). As expected, inhibition of this pathway drastically reduced pS6$_{(235/236)}$ levels, compared to the vehicle controls at the two-hour time point (Fig. 4, *C* and *D*). Despite the reduction in pS6 caused by each of the drugs, it is notable that although T cells treated with MK2206 or rapamycin displayed lower pS6$_{(235/236)}$ levels, that did not translate to increased TrIP expression, in contrast to what we seen in cells treated with IC87114 (Fig. 4, *C* and *D*). Taken together, these data do not support the hypothesis that TrIP surface expression is regulated *via* an autocrine PI3K-pathway related mechanism.

We next expanded the scope of these experiments to include inhibitors targeting a broader range of signaling pathways. This included inhibitors of calcium signaling (FK-506; calcineurin inhibitor), ERK (U0126; MEK1/2 inhibitor), and dasatinib (Src family kinase inhibitor). Perhaps unsurprisingly, the potent inhibition of upstream kinases by dasatinib (which would include Lck) resulted in broad inhibition of TCR signaling and significant preservation of TrIP expression (>50%) at 2 h after stimulation (Fig. 4, *E* and *F*). Although, importantly, dasatinib treatment at this dose did not completely prevent T cell activation and TrIP loss, as we still observed complete TrIP loss at the four-hour time point, similar to the vehicle group (Fig. 4, *E* and *F*). Moving further downstream of the TCR, we found that inhibition of either calcineurin or MEK1/2 activity under these conditions also led to significant preservation of TrIP expression (at least 60% and 40% of starting levels, respectively) in CD8$^+$ T cells following 2 h of stimulation, compared to around 18% in the untreated control (Fig. 4, *E* and *F*). While these compounds had statistically significant effects on TrIP expression, they did not detectably impact pS6$_{(235/236)}$ levels (Fig. 4, *G* and *H*). These results suggest that while calcium and ERK-MAPK signaling play critical roles in regulating TrIP downregulation, there is also a contribution, although more minor, of the PI3K pathway itself.

In addition to calcium (Ca^{2+}) and PIP_3, another critical second messenger downstream of TCR signaling is diacylglycerol (DAG), which functions in part to activate several isoforms of PKC. The PKC family of serine/threonine kinases comprises three major classes based on their physiological activators. The classical PKCs (α, βI, βII, and γ) and the novel PKCs (δ, ε, η, and θ) both require DAG for activation, but while the classical PKCs also require Ca^{2+} the novel PKCs do not (24). By contrast, so-called atypical PKCs (ζ and λ/ι) require neither DAG nor Ca^{2+} for activation (24). Since PKCs are connected to both calcium and ERK signaling, we hypothesized that one or more PKC family members may play a key role in regulating TrIP downregulation.

Given the complexity of the PKC family, we started our survey with pan-PKC inhibitors, including bisindolylmaleimide I (Bis I), sotrastaurin, and Gö6983. Thus, we found that broad pharmacological inhibition of PKC activity resulted in nearly complete prevention of TrIP downregulation from P14 T cells at 2 h after peptide stimulation (Fig. 5, *A* and *B*). Although these inhibitors share similar activities against the various PKC family members, they resulted in somewhat different kinetic effects on downregulation of TrIP and induction of pS6 (Fig. 5, *C* and *D*), which could be due to differential off-target effects of the compounds. To better discriminate between the role of classical (α, βI, βII, and γ) and novel PKCs (δ, ε, η, and θ) in TrIP downregulation we treated T cells with Go6976, a PKC inhibitor with high selectivity for classical PKC's and little activity against PKCθ (25), the predominant PKC activated by the TCR (26, 27). Treatment with Go6976, similar to the other PKC inhibitors, also led to significant inhibition of TrIP

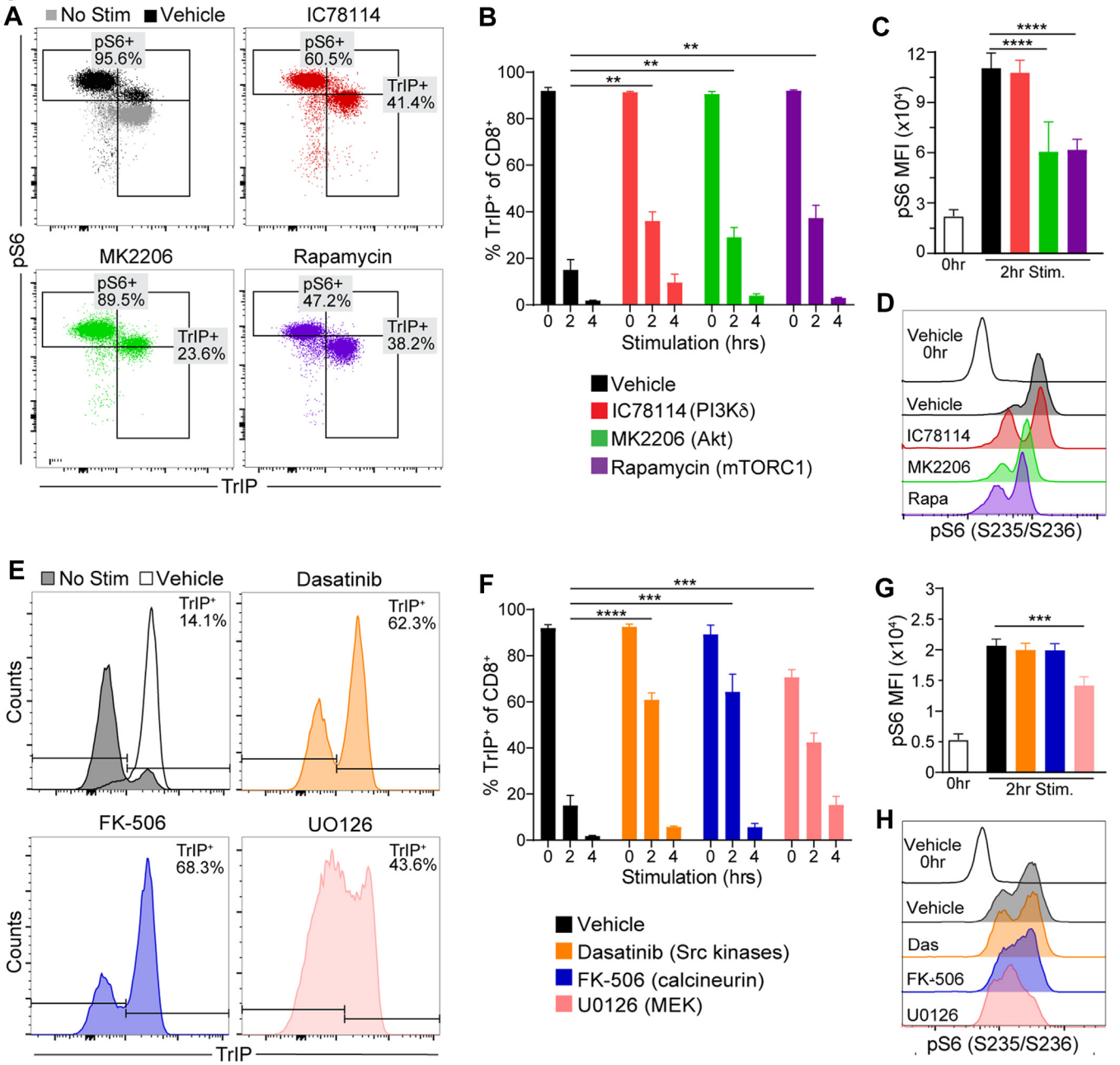

Figure 4. The PI3K pathway is dispensable for TrIP downregulation. WT P14 splenocytes were pretreated for 30 min with the indicated inhibitors and then stimulated with 200 ng/ml cognate WT gp33 peptide, still in the presence of inhibitor. TrIP loss on the $CD8^+$ T cells was followed over time by flow cytometry. *A*, dot plots showing $pS6_{(S235/S236)}$ *versus* TrIP expression on the $CD8^+$ T cells at the 2-h time point. *B*, quantification of TrIP expression at each time point for each treatment *C*, quantification of $pS6_{(S235/S236)}$ MFI at the 2-h time point, with 0 h values as comparison. *D*, representative histograms of $pS6_{(S235/S236)}$ staining at the 2-h time point, with 0-h histogram as comparison. *E*, representative histograms of TrIP expression at the 2-h time point following stimulation. *F*, quantified summary of TrIP expression at each time point for each treatment. *G*, quantification of pS6 levels at the 2-h time point, with 0-h values as comparison. *H*, representative histograms of pS6 staining at the 2-h time point with 0-h histogram as comparison. Ordinary two-way ANOVA was applied for statistical comparisons (*p*: *<0.05, **<0.01, ***<0.001, ****<0.0001). MFI, mean fluorescence intensity; pS6, phosphorylation of the S6 ribosomal subunit; TrIP, transmembrane inhibitor of PI3K.

downregulation, compared to vehicle control (Fig. 5, *A* and *B*)). These data suggest that PKCθ activity alone is insufficient to trigger comparable degrees of TrIP downregulation. Together, these data suggest that PKCs play a major role in regulating the surface downregulation of TrIP following TCR stimulation. While both classical and novel PKCs may contribute to TrIP cleavage, our data suggest that classical PKCs play a more predominant role in this process.

Role of metalloproteases in acute TrIP downregulation

While the above data further define the cellular signaling prerequisites for TrIP downregulation, we have yet to fully understand the direct mechanism by which TrIP is lost. Shedding of surface proteins by proteolytic cleavage has been shown to play numerous immunological roles, with the ADAM (A disintegrin and metalloproteinase domain-containing) family of proteases playing prominent roles

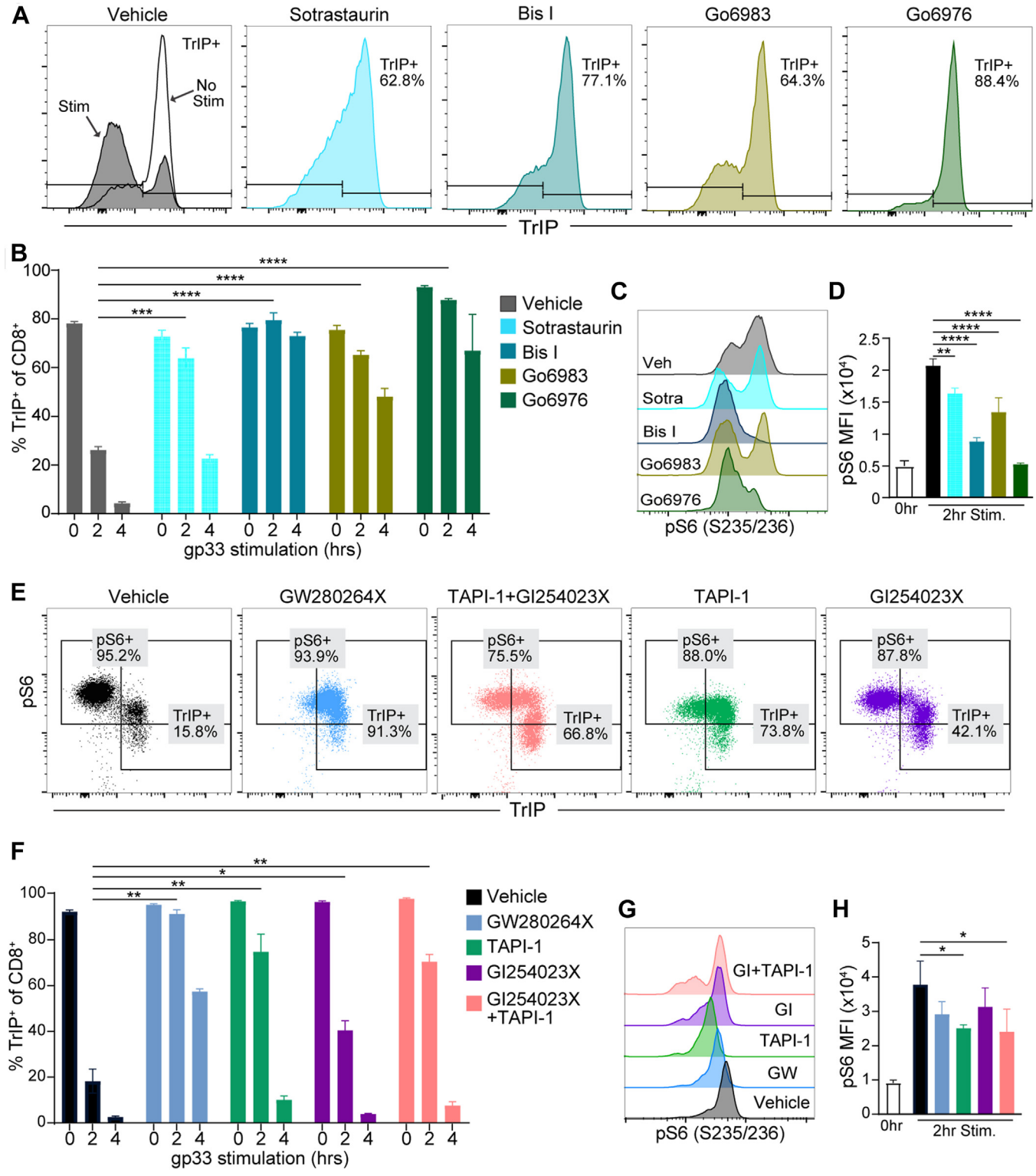

Figure 5. PKC and ADAM17 activity are required for downregulation of cell-surface TrIP. WT P14 splenocytes were stimulated with 200 ng/ml WT gp33 peptide in the presence of the indicated inhibitors. TrIP loss on the $CD8^+$ T cells was followed over time by flow cytometry. *A*, flow plots of TrIP staining in each PKC inhibitor treatment at 2-h time point following stimulation. *B*, quantification of TrIP expression at each time point for each PKC inhibitor treatment. *C*, representative histograms of $pS6_{(S235/S236)}$ staining at the 2-h time point. *D*, quantification of $pS6_{(S235/S236)}$ MFI at the 2-h time point. *E*, representative flow plots $pS6_{(S235/S236)}$ *versus* TrIP expression treatment at the 2-h time point in the presence of ADAM inhibitors. *F*, quantification of TrIP expression across each ADAM inhibitor treatment. *G*, representative histograms of $pS6_{(S235/S236)}$ staining at the 2-h time point. *H*, quantification of pS6(S235/S236) MFI at the 2-h time point. Ordinary two-way ANOVA statistical analysis applied for statistical comparison (*p*: *<0.05, **<0.01, ***<0.001, ****<0.0001). MFI, mean fluorescence intensity; PKC, protein kinase C; pS6, phosphorylation of the S6 ribosomal subunit; TrIP, transmembrane inhibitor of PI3K.

(28–30). In fact, our initial studies using expression of Flag-tagged murine TrIP constructs in T cells (16) revealed that the inhibitor GW280264X ("GW," a dual inhibitor of ADAM10/ADAM17) prevented stimulation-induced downregulation of TrIP (16). Thus, we sought to evaluate if endogenous murine TrIP is regulated in a similar manner. Expanding on our previous work, we set out to determine the relative contributions of ADAM10 versus ADAM17 in the cleavage of TrIP from the surface. In addition to the ADAM10/17 dual inhibitor (GW), we also used GI254023X (GI) an ADAM10 inhibitor with 100-fold selectivity for ADAM10 over ADAM17. There are limited specific inhibitors for ADAM17 that do not interfere with ADAM10, but using TAPI-1 we could at least preferentially target ADAM-17, as it has a 10-fold lower potency for ADAM10. As shown in Figure 5, *E* and *F*, potent inhibition of both ADAM10/17 (using GW) resulted in significant preservation of TrIP expression following stimulation. ADAM17 inhibition by TAPI-1 appeared to more significantly preserve cell-surface TrIP (20% loss) compared to the ADAM10-inhibited (GI) group (40% loss) (Fig. 5, *E* and *F*). Furthermore, when we combined these compounds, the effect was not additive, instead mimicking inhibition with TAPI-1 alone (Fig. 5, *E* and *F*). Finally, these experiments reinforced our understanding of negative regulation of PI3K by TrIP, as conditions in which TrIP expression was maintained also had lower levels of pS6 induction (Fig. 5, *G* and *H*), consistent with maintenance of TrIP-mediated PI3K inhibition. Together, these data confirm that downregulation of cell-surface TrIP expression in $CD8^+$ T cells is mediated, at least in part, by ADAM10 and ADAM17.

Given the limitations of the pharmacological tools, we next sought to deconvolute the relative contributions of ADAM10 *versus* ADAM17 to the cleavage of TrIP from the cell surface, as well as further define the role of PKC activity in this pathway. We thus used CRISPR/Cas9 to target ADAM10, ADAM17, and PKCθ. While both pharmacologic and genetic approaches can result in off-target effects, additional genetic confirmation of the above data would strengthen our understanding of the mechanisms of TrIP expression regulation. Two crRNAs per gene were designed to target to the genes encoding PKCθ, ADAM10, and ADAM17 (see Experimental procedures). There are several challenges with targeting genes *via* CRISPR in naïve T cells, as most protocols involve prior or concurrent activation of the T cells. We felt it was critical to use naïve $CD8^+$ T cells for these experiments, to be consistent with the experiments described above and given that stimulation through the TCR causes acute downregulation of TrIP. Based on a published protocol, we used beads to isolate naïve CD8 T cells and incubated them in rIL-7 for 24 h prior to nucleofection (31, 32). These T cells were then cultured in IL-7 for an additional five-to-seven days, prior to stimulation, to allow for turnover of message and protein.

Using this approach, we achieved robust downregulation of ADAM10 by day five in culture, as shown by the flow plots in Figure 6*A*. We discovered CRISPR KO of ADAM10 in naïve CD8 T cells resulted in a significant increase in baseline TrIP expression by mean fluorescence intensity (Fig. 6, *A* and *B*), suggesting that ADAM10 plays a role in constitutive shedding of endogenous TrIP. Additionally, ADAM10 KO led to a modest, but statistically significant, attenuation of the overall degree of TrIP downregulation following TCR stimulation, at the level of overall TrIP mean fluorescence intensity (Fig. 6, *C* and *D*). We observed a similar effect when quantifying the percentage of cells falling into the $TrIP^+$ gate after stimulation (Fig. 6*I*). These data provide additional evidence that ADAM10 plays a role in both constitutive and inducible TrIP downregulation, *via* cleavage. These data are in line with the literature, as ADAM10 has been shown to be responsible for both constitutive and also induced and/or regulated shedding of other proteins as well (33, 34). Next, we sought to KO ADAM17 in naïve T cells using the same approach. However, despite designing multiple guide RNA's and other protocol modifications, we were not able to detectably alter the expression of ADAM17 in naïve $CD8^+$ T cells following CRISPR-targeted KO (not shown). While this could be due to multiple reasons, we believe ADAM17 protein turnover and/or degradation had not occurred, despite testing for ADAM17 KO up to 10 days following electroporation. This idea is supported by the literature, as lysosomal degradation of mature ADAM17 has been shown to require PKC activation (35), consistent with the lack of ADAM17 turnover that we observed.

We next turned our attention back to PKCθ, using the CRISPR approach. Thus, we were able to achieve a marked, although incomplete (∼60%), reduction in PKCθ staining (Fig. 6*F*). However, we did not observe an increase in the baseline level of TrIP upon PKCθ KO (Fig. 6*G*) like we saw in the ADAM10 KO, even when gating specifically on $PKC\theta^+$ *versus* $PKC\theta^-$ cells, suggesting that PKCθ is not required for the constitutive shedding of TrIP. Consistent with this finding, we also did not observe any effect of PKCθ KO on stimulation-dependent TrIP downregulation (Fig. 6, *G*, *H*, and *J*), again even when gating on $PKC\theta^+$ *versus* $PKC\theta^-$ cells in the WT and KO samples, respectively. These data indicate that, although PKCθ is the major isoform of PKC linked to many TCR signaling-dependent events, other PKC family members play more dominant roles in the downregulation of TrIP, consistent with the above pharmacological data.

Structural requirements for TrIP downregulation

Next, we wanted to understand where in the ecto domain of TrIP the ADAM-mediated cleavage occurs. We focused on the 76-amino acid long connecting "stalk domain" linking the extracellular kringle domain to the transmembrane and intracellular domains (Fig. 7*A*). Assessment of the putative structure of this protein in AlphaFold (36, 37) suggests that the extracellular "stalk" domain region of TrIP is unstructured in nature (Fig. 7*A*). Initially, we explored *in silico* prediction methods (*e.g.*, iProt-Sub) to identify predicted metalloprotease cleavage sites (38). This analysis revealed multiple possible sites of cleavage, which spanned a wide range of the stalk domain (Fig. 7*A*), and thus did little to narrow down the region(s) where cleavage might occur. The shortcomings of these

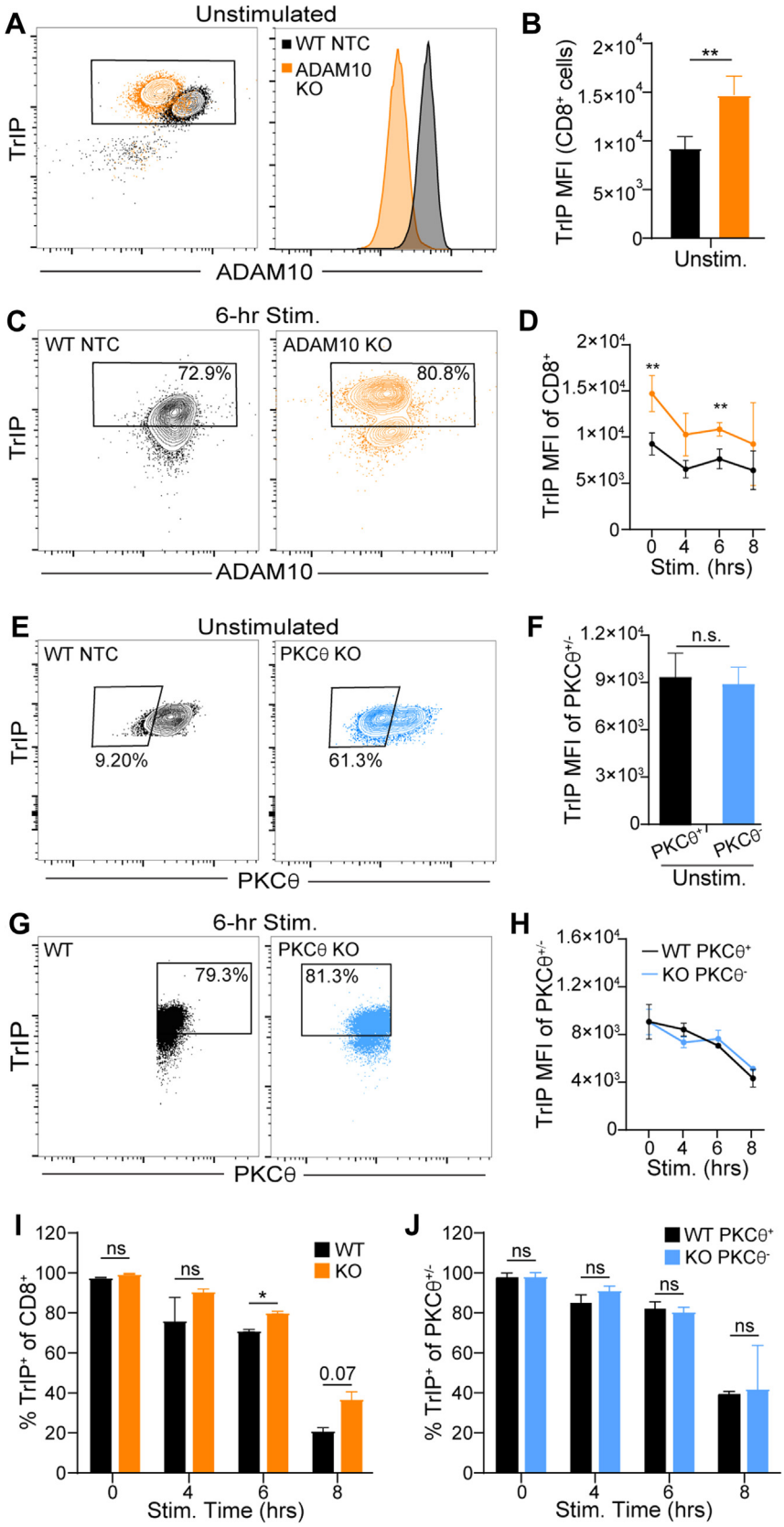

Figure 6. CRISPR-mediated KO in naïve CD8 T cells confirms a role for ADAM10 in TrIP downregulation and suggests that PKCθ is dispensable. Naïve T cells were transfected with Cas9 ribonucleoprotein's targeting ADAM10 or PKCθ, then maintained in rIL-7 for 7 days *in vitro*, followed by stimulation with α-CD3 mAb. *A* and *B*, KO efficiency of ADAM10, shown by flow cytometry (*A*) and histogram (*B*), which indicate an increase in basal TrIP expression before stimulation. TrIP expression was assessed on day 7 after nucleofection, prior to stimulation. *C* and *D*, expression of TrIP and ADAM10 after stimulation of the indicated cells, at the indicated time points. Samples were gated on total $CD8^+$ cells. *E* and *F*, expression of PKCθ and TrIP at day 7 after nucleofection,

types of prediction are due to the somewhat promiscuous target specificity of ADAM metalloproteases (39, 40). Previous reports suggest that ADAM mediated cleavage typically occurs in sites proximal to the cell membrane (41), so we focused on that area of TrIP. We therefore made a series of internal deletion mutants to confirm, that both, cleavage is the mechanism by which cell-surface TrIP is downregulated and also to create a noncleavable TrIP construct for future functional studies. The sites of these deletions are indicated in Figure 7*B*; each construct also included a Flag-tag for detection. Thus, when we stimulated D10 T cells expressing both WT and our truncated TrIP constructs, deletion of just a 16 amino acid sequence (Δ16aa) was not sufficient to prevent cleavage/loss (Fig. 7, *D* and *E*). By contrast, there was no detectable cleavage of a TrIP construct with a more substantial 29 amino acid deletion (Δ29aa; Fig. 7*F*). Corroborating earlier results, the inability to cleave Δ29aa TrIP construct from the cell surface led to increased basal TrIP expression (Fig. 7*G*), similar to the ADAM10 KO data discussed above. It is still unclear whether this is due to enhanced production or processing of the transfected protein or whether it might be the result of diminished steady-state cleavage of TrIP.

As described above, our data suggested that PKC activation is required for downregulation of cell-surface TrIP, so we also stimulated transfected D10 T cells with phorbol 12-myristate 13-acetate (PMA), which directly activates multiple PKC isoforms (35, 42). The potent stimulation mediated by PMA led to near complete loss of both WT and Δ16 TrIP within 1 h of treatment. Strikingly however, the Δ29aa mutant was still resistant to downregulation, even in the presence of PMA (Fig. 7, *F* and *G*). Consistent with our previous study (16) and data shown above, expression of the cleavage-resistant Δ29 form of TrIP led to a decrease in pS6 staining in TCR-stimulated D10 T cells (Fig. 7*F*). Together, these data expand our understanding of TrIP regulation, showing that TrIP cleavage from the surface by ADAM17 (TACE) occurs in the stalk region, between residues 120 and 133, and that in the absence of TrIP downregulation, partial suppression of the PI3K/Akt pathway is maintained.

Discussion

In this study, we expand on the understanding of TrIP, a transmembrane protein comprised of an extracellular protein-protein interaction kringle domain (43, 44), and an intracellular "p85-like" domain (15, 16, 18). The p85-like domain of TrIP has been shown to interact with the p85/p110 heterodimer of PI3K and negatively regulate its catalytic activity, although this is not a complete inhibition (18). Furthermore, expression of TrIP in T cells has been shown to negatively regulate their activation and that its deletion can enhance their inflammatory activities (15, 16). While gaining valuable insight into fundamental TrIP biology, these previous studies were hindered by the lack of availability of a robust anti-murine TrIP mAb and thus relied on cell line expression systems and knock-out/knock-down to characterize its function. In this study, we describe the production and validation of three novel anti-mTrIP IgG monoclonal antibodies capable of recognizing endogenous murine TrIP protein for detection by flow cytometry. There is relatively high sequence homology (>80%) between mouse and human TrIP, and while not all mAb clones were capable of cross-reactivity we do find that the top clone (18E10) can detect both human and murine TrIP. Each of the three clones appears to stain TrIP *via* its kringle domain, since deletion of that domain completely abrogated staining.

Consistent with publicly accessible gene expression data, splenic T and B lymphocytes demonstrated some of the highest levels of TrIP protein expression. Nonetheless, we also observed relatively high expression of TrIP on neutrophils, something that has not yet been reported in the literature. Furthermore, upon subsetting CD8 T cells based on CD44 *versus* CD62L expression, we found that the naïve CD62L$^+$ cells comprise the majority of the TrIP-expressing cells, whereas it was not detectable on CD44$^+$ cells. We further showed that this endogenous TrIP expression on naïve CD8$^+$ T cells is lost within the first few hours after TCR stimulation, confirming our previous studies with the D10 helper T cell line (16). Building upon these data, we found that TrIP expression is lost following stimulation with anti-CD3 mAb or peptide antigen in a dose-dependent manner. Furthermore, this loss appears to be largely independent of the "signal 2" (CD28) contribution, as blockade with CTLA4-Ig had little-to-no effect. While having confirmed previous studies that suggested TrIP expression would be found on naïve T cell populations and lost upon activation, it was unclear when, or even if, TrIP may be reexpressed following T cell activation. Our results show that although TrIP expression does remain low for up to 12 h following activation, T cells do begin to reexpress TrIP by 24 h, at least *in vitro*. This re-expression of TrIP suggests it may play a previously unexplored role in longer lived populations like memory T cells, a subject that is worthy of further study.

The ability to track endogenous TrIP protein on T cells has given us a new understanding of how TrIP expression may coordinate early T cell activation signals. Ours is the first study, that we know of, to describe an early activation state in CD8$^+$ T cells during which TrIP is still expressed and there is an intermediate level of PI3K activation (as read-out by pS6). This temporally correlated series of signaling events adds to our understanding of the complex role of TrIP in early T cell activation. Along with the kinetics of S6 phosphorylation, we also found that upregulation of CD69, a well-characterized marker of early T cell activation (45), was inversely correlated with the downregulation of TrIP.

and before stimulation, shown by flow cytometry (*E*) and histogram (*F*). MFI data in panel F are from the PKCθ$^+$ or PKCθ$^-$ gate in panel G for WT and KO cells, respectively. *G* and *H*, expression of TrIP and PKCθ after stimulation of the indicated cells, at the indicated time points. MFI data in panel H are from the PKCθ$^+$ or PKCθ$^-$ gate in panel G for WT and KO cells, respectively. *I* and *J*, the percentage of TrIP$^+$ cells at the indicated time points after stimulation. Cells in panel I (ADAM10 KO) were gated on total CD8$^+$ cells; cells in panel J were gated on PKCθ$^+$ or PKCθ$^-$ cells in WT and PKCθ KO conditions, respectively. Ordinary two-way ANOVA was used for statistical comparisons (*p*: *<0.05, **<0.01, ***<0.001, ****<0.0001). mAb, monoclonal antibody; MFI, mean fluorescence intensity; PKC, protein kinase C; TrIP, transmembrane inhibitor of PI3K.

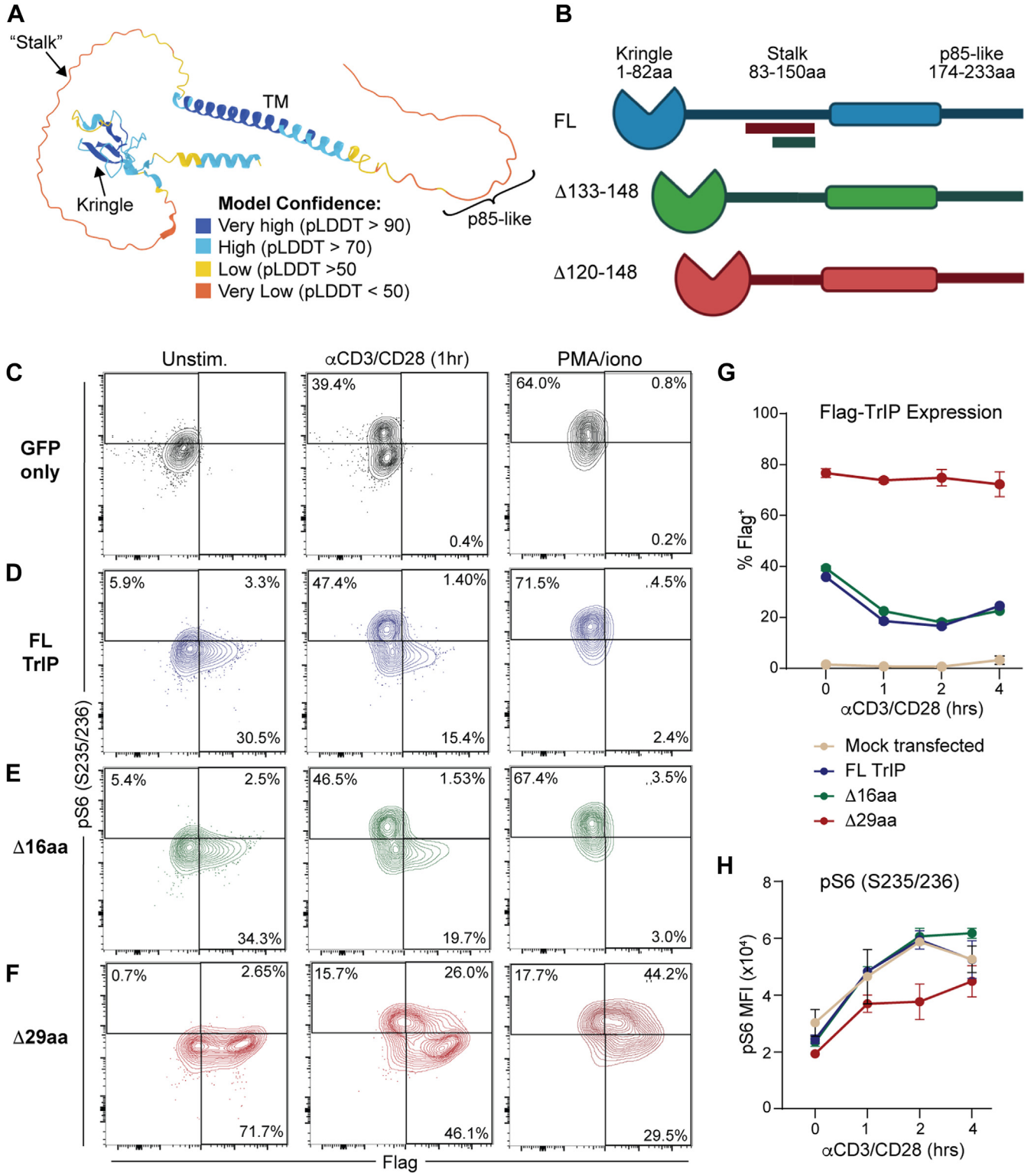

Figure 7. Truncation of the extracellular stalk renders TrIP resistant to cleavage and dampens PI3K signaling. D10 T cells were cotransfected with pMaxGFP alone or together with the indicated TrIP plasmid constructs. Twenty-four hours following transfection, cells were stimulated with 10 μg/ml plate-coated anti-CD3 + anti-CD28 or PMA/ionomycin (50 ng/ml and 500 ng/ml, respectively). *A*, AlphaFold sourced predicted crystal structure of TrIP protein, indicated is the model confidence by color. *B*, diagram depicting the two truncation mutants used in these studies. All flow plots show cells gated on GFP$^+$. *C*, control GFP-only transfected D10 cells (GFP only) depicted without stim, following 1-h of stimulation with αCD3/CD28 or PMA/ionomycin. *D*, Co-GFP+WT TrIP (FL TrIP) transfected D10 T cells depicted without stimulation, or following 1-h ofstimulation with αCD3/CD28 or PMA/ionomycin. *E*, D10 T cells cotransfected with GFP and the Δ16aa mutant of TrIP (16aa del'n) depicted without stim, or following 1-h of stimulation with αCD3/CD28 or PMA/ionomycin. *F*, D10 T cells cotransfected with GFP + the Δ29aa mutant of TrIP (29aa del'n) depicted without stimulation or following 1-h of stimulation with αCD3/CD28 or PMA/ionomycin. *G*, quantification of TrIP-Flag (%Flag$^+$) in transfected D10 cells following αCD3/CD28 stimulation. *H*, quantification of pS6$_{(235/236)}$ MFI in the transfected D10 cells following αCD3/CD28 stimulation. MFI, mean fluorescence intensity; PMA, phorbol 12-myristate 13-acetate; pS6, phosphorylation of the S6 ribosomal subunit; TrIP, transmembrane inhibitor of PI3K.

We also studied the relationship of TrIP downregulation to TCR signaling. While TCR ligation triggers multiple signaling pathways, we initially focused on the PI3K pathway, as we had observed a relationship between the loss of TrIP and the upregulation of pS6. By pharmacologically targeting various members of the PI3K pathway, we found that regardless of which stage of the pathway was inhibited, each resulted in small but consistent effects, *i.e.* slower kinetics of TrIP downregulation. These relatively minor effects may be a result of lower available PIP_3 and/or active Akt, which can participate in parallel signaling pathways (46). For example, PIP_3 promotes the activation of Itk, leading to enhanced PLC-γ1 activation and Ca^{2+} signaling; in addition, calmodulin is known to compete with Akt for PIP_3 (46). Thus, this led to our expansion of the investigation to other pathways and we found that inhibition of enzymes more proximal to calcium signaling (calcineurin) or ERK activity (MEK1/2) had much greater impacts on the kinetics of TrIP loss.

The above data also led us further explore the roles of the PKC family of enzymes, as some members of this family are activated in a Ca^{2+}-dependent manner and are known to promote activation of MAPK signaling (29, 47). We found that broad inhibition of PKC activity significantly inhibits the downregulation of TrIP following T cell activation, suggesting a major role in directing its cleavage from the cell surface. Although the novel isoform PKCθ is thought to be the major isoform linking TCR signaling to downstream MAPK and NF-κB signaling (48, 49), TCR stimulation is associated with activation of classical and other PKC isoforms (50). Employing Go6976, an inhibitor selective for classical PKC's (thus leaving PKCθ activity largely intact), we again observed robust inhibition of TrIP loss following stimulation. These data suggest a primary role for classical PKCs in triggering TrIP cleavage, with the caveat that there are additional off-target effects of this compound (*e.g.*, on other calcium-dependent kinases) (25). To more directly address the role of PKCθ, we used CRISPR-mediated KO in naïve $CD8^+$ T cells. While we were able achieve a significant degree of knockout of PKCθ in the majority (>60%) of naïve T cells, there was no significant effect on TrIP expression before or after stimulation, even when gating specifically on cells lacking PKCθ expression. In aggregate, our pharmacological and CRISPR KO data suggest that the classical PKC isoforms are primarily responsible for inducible downregulation of TrIP in T cells.

Building on previous studies, we obtained pharmacological evidence for ADAM10 and ADAM17 being the major proteases responsible for downregulation (likely *via* cleavage) of endogenous TrIP in $CD8^+$ T cells. While we were able to corroborate the role of ADAM10 *via* CRISPR-mediated KO, the contribution of ADAM17 was difficult to define with this approach. Nonetheless, together our findings are consistent with reports showing extensive overlap between ADAM10 and ADAM17 substrates (51–53). The cleavage of cell surface proteins by ADAM proteases typically occurs in close proximity to the plasma membrane. Thus, to better define the site of TrIP cleavage, we produced TrIP constructs with truncated "stalks." Dramatically, removal of a 29-amino acid region of the extracellular domain (residues 120–148) completely abrogated the downregulation of TrIP following activation, while a shorter deletion of this same region had no detectable effect. These data suggest that the cleavage site lies within that region, although it is formally possible that shortening the length of this region results in steric hindrance of activated ADAM access to the cleavage site. Of note, the noncleavable (29AA deletion) construct displayed higher baseline expression of TrIP when compared to WT constructs, suggesting that TrIP is subject to low rates of basal shedding, even in the absence of TCR stimulation. We also observed an increase in basal TrIP expression in ADAM10 KO T cells, suggesting that constitutive shedding of TrIP may be driven (at least in part) by ADAM10-mediated cleavage in this region. Further investigation is needed to fully define the specific cleavage site and to understand the role that shedding of TrIP has on *in vivo* T cell activation and differentiation, similar to studies defining the role of other immunomodulatory molecules such as Lag3 and Tim-3 (52, 54).

We have yet to directly address the fate of the TrIP cytoplasmic tail following ecto domain cleavage. Thus, the cytoplasmic portion of TrIP contains a "p85-like domain," which is reported to inhibit the catalytic activity of PI3K (16). Of note, none of the commercially available antibodies against the C terminal portion of TrIP were suitable for these studies, as they did not yield specific or robust enough signals when tested. However, our previous work used a series of Flag-tagged TrIP constructs in cell line expression systems, revealing that removing either the extracellular (Δkringle) or the intracellular (Δp85-like) domains abrogated the inhibitory activity of TrIP (16). Furthermore, in the absence of the kringle domain, cells maintained expression of the Flag-tagged intracellular TrIP domain following stimulation, suggesting that the intracellular p85-like domain of TrIP persists for some time. We thus hypothesized that the kringle domain is required for TrIP localization proximal to the TCR, and that cleavage of the extracellular domain enables its exclusion from TCR synapse following activation. More studies are needed to fully define these mechanisms with endogenous TrIP protein, as the currently available tools limit many of these studies to cell line expression systems.

In summary, we present data expanding our understanding of the relationship of PIK3IP1/TrIP to signals that regulate T cell activation. Future studies on the downstream effects of TrIP downregulation in specific disease contexts are still needed to fully understand the impact of TrIP regulation in the T cell compartment. TrIP itself represents a potentially unique biological target, as preventing its inhibition in T cells could improve responses to cancer or infection, whereas strategies to prevent its downregulation may help suppress autoimmunity or chronic inflammation.

Experimental procedures

Antibodies and flow cytometry

For extracellular staining, single cell suspensions were stained at 4 °C for 30 min with Live/Dead + antibody cocktail containing anti-CD16/CD32 (Fc Shield; Tonbo Biosciences:

clone 2.4G2) resuspended in PBS. For intracellular staining, cells were fixed/permeabilized using the eBioscience Foxp3/transcription factor staining buffer set (00–5523–00), as per manufacturer instructions. Following fixation, intracellular staining antibodies were resuspended in 1x permeabilization buffer and used to stain at 4 °C for 30 min.

The following antibodies and dyes were used for these analyses: anti-CD90.2 (BD Biosciences; clone 53–2.1), anti-CD8α (BD Biosciences; clone 53–6.7), anti-CD44 (BD Biosciences; clone IM7), anti-CD11c (BD Biosciences; clone N418), anti-TCRβ (BD Biosciences; clone H57–597), anti-CD4 (BioLegend; clone RM4-5), anti-CD11b (Thermo Fisher Scientific: clone M170), anti-CD62L (BioLegend; clone MEL-14), anti-F4/80 (BioLegend; clone BM8), anti-CD25 (BD Biosciences: clone 7D4), anti-Gr-1 (Invitrogen: clone RB6-8C5), anti-CD19 (BioLegend: clone 1D3), anti-Foxp3 (Invitrogen; FJK-16s), anti-pS6$_{(235/236)}$ (Cell Signaling; clone D57.2.2E), anti-TCR Vα2 (Biolegend; clone AF-7), anti-CD69 (BioLegend: clone H1.2F3), anti-Flag (BioLegend; clone L5). Live/dead staining was performed using the Zombie NIR fixable viability kit (BioLegend; 423105). For the CRISPR KO studies, we additionally used anti-PKCθ (Cell signaling; clone E1I7Y) and anti-ADAM10 (R&D; clone # 139712) for staining. Alexa Fluor 488 Anti-Rabbit IgG was used as a secondary against PKCθ (Jackson ImmunoResearch; Cat No. 711-545-152) and Goat anti-Rat IgG Alexa Fluor 488 (Invitrogen; Cat No. A-11006).

For the majority of TrIP staining experiments, the 18E10 clone showed the most robust and reproducible staining and was therefore used for the studies involving endogenous murine TrIP. We directly conjugated the α-TrIP 18E10 to Alexa Fluor 647 using a commercial labeling kit (Invitrogen A20186), per manufacturer's instructions. All flow cytometry was performed on a 5-laser Cytek Aurora and flow cytometry data were analyzed with FlowJo (v10.10.0; https://www.flowjo.com).

Animals

All experiments involving animals were approved by the University of Pittsburgh Institutional Animal Care and use Committee (IACUC). We previously generated a conditional mouse KO strain with LoxP sites inserted into the TrIP gene (*Pik3ip1*$^{fl/fl}$), targeting the removal of exons 2 to 5 (16). These mice were crossed to E8i^{cre} mice (Jackson strain #008766), to achieve KO of *Pik3ip1* specifically in CD8$^+$ T cells. For peptide stimulation studies, we used the P14 TCR transgenic strain that expresses a TCR specific for the gp33 peptide from LCMV (Jackson; Strain #037394). All strains were backcrossed more than nine generations to C57BL/6J (Jackson; Strain #000664). Mice were bred in-house under specific-pathogen-free conditions, and experimental mice were either littermates or housed in the same facility and same room. Experiments were conducted on mice 6 to 8 weeks of age, with age and sex-matched groups.

Generation of TrIP-Ig fusion protein

To generate the TrIP-Ig fusion, the ecto domain of murine TrIP/Pik3ip1 was PCR amplified from IMAGE consortium clone number 4039129, using primers to add EcoRV and BglII sites at the 5′ and 3′ ends, respectively. This fragment was then cloned into the same restriction sites of pFuse-hIgG1-Fc2. Reading frame and integrity of the cloned fragment were confirmed by sequencing. This plasmid was then transfected into HEK293T cells and Protein-A purified by a commercial vendor (Syd Labs, Inc).

Development of mAb's to the ecto domain of TrIP

Monoclonal antibodies to the ecto domain of murine TrIP were developed in conjunction with a commercial vendor (Rockland, Inc). Briefly, Sprague-Dawley rats were immunized with the aforementioned TrIP-Ig fusion protein. Immunized rat splenocytes were then fused with Sp2/0-Ag14 myeloma cells to generate hybridomas. These hybridomas were subsequently subcloned one or more generations *via* limiting dilution. Reactivity/specificity of each was initially screened *via* ELISA for reactivity with recombinant TrIP-Ig protein, and counter-screened against human IgG1.

Generation of TrIP deletion mutant constructs

For the initial antibody validation experiments, full-length human *PIK3IP1* and full-length mouse *Pik3ip1* gBlocks (IDT) were cloned into pcDNA3.1 *via* restriction enzyme cloning. For TrIP cleavage experiments, two truncated and one full-length TrIP gBlocks (IDT) were produced and cloned into a minimal pcDNA3.1(+) backbone modified from pcDNA3.1(+) (Invitrogen). In the first TrIP truncation, a 16 amino acid sequence was removed [AA positions 133–148; (DNA sequence: CAGTCAGCTTGTGAGGATGAACTCCAAGGAAAAAAAAGACCTAGGAAC)]. For the second truncation, that deletion was extended an additional 13 amino acids to make a 29 amino acid deletion [AA positions 120–148 removed; (DNA sequence: AGGAGTGAGGCAGCCGAGGTGCAGCCAGTGATCGGGATCAGTCAGCTTGTGAGGATGAACTCCAAGGAAAAAAAAGACCTAGGAAC)]. Each construct used for transfections was designed to include a Flag tag (DYKDDDDK) for antibody recognition *via* anti-Flag antibody (clone: L5). All plasmid constructs' multiple cloning sites were verified by Sanger sequencing.

Cell lines, transfections, and activations

Human embryonic kidney (HEK) 293T cells were cultured in Dulbecco's modified Eagle's medium containing 10% bovine growth serum (BGS; Hyclone), 1 % penicillin/streptomycin, and 1% L-glutamine. D10.G4.1 mouse T helper cell line (D10 cells) were maintained in 50 U/ml rhIL-2 in complete RPMI (cRPMI) media (cRPMI supplemented with 10% BGS, 1% penicillin/streptomycin, 1% L-glutamine, 50 mM 2-mercaptoethanol, 1x nonessential amino acids, 1% Hepes, and 1% sodium pyruvate). Transfection of HEK293T cells was performed using TransIT-LT1 (Mirus Bio; MIR 2304) per manufacturer instructions. Transfection of D10 cells *via* electroporation was performed using a Bio-Rad Gene Pulser Xcell (Square Pulse protocol; 400V, 3 pulses, 0.5 ms pulse length, 0.05 s between pulses). For truncated TrIP expression experiments, pMaxGFP was cotransfected as a positive control

(Lonza Biosciences). Activation of D10 cells was *via* plate-coated anti-CD3 (clone:145-2C11; Tonbo Biosciences 50–201–4837); anti-CD28, (clone 37.51; BioLegend: 102101).

Mouse tissue processing and in vitro *stimulation*

Spleens harvested from either WT C57BL/6J or WT P14 TCR Tg mice were mechanically disrupted and filtered to single cell suspensions. Red blood cells were removed *via* 1x RBC lysis buffer (eBioscience 00-4333-57), according to the manufacturer's instructions. Splenocyte stimulations were performed in complete RPMI (cRPMI) media (cRPMI supplemented with 10% BGS, 1% penicillin/streptomycin, 1% L-glutamine, 0.05 mM 2-mercaptoethanol, 1x nonessential amino acids, 1% Hepes, and 1% sodium pyruvate). Anti-CD3 (clone:145-2C11; Tonbo Biosciences 50–201–4837); and anti-mCD28, clone 37.51; BioLegend: 102101) were used for plate-coating at the indicated concentrations. For P14 TCR Tg stimulations, three different peptides were selected based on published work by Boulter *et al.* (23); a high affinity gp33 peptide (sequence: KAVYNFATM), the WT gp33 peptide (sequence: KAVYNFATC), and a peptide with lower affinity, L6F gp33 (sequence: KAVYNLATC).

Inhibitors

For the *in vitro* TrIP downregulation experiments, inhibitors used were as follows: IC87114 (Selleckchem; S1268), 10 μM; MK-2206 (Cayman Chem; 11593), 2.5 μM; rapamycin (Selleckchem; S1039), 100 nM; dasatinib (Stemcell; 73082), 2.5 nM; FK-506 (Selleckchem; S5003), 10 μM. U0126 (MedChemExpress; HY-12031), 2.5 μM; bisindolylmaleimide I (Selleckchem; S7208), 10 μM; sotrastaurin (Selleckchem; S279101), 5 μM; Go6983 (MedChemExpress; HY-13689), 2.5 μM; Go6976 (MedChemExpress; HY-10183) 1.25 μM GW280264X (Bio-Techne; Cat# 7030), 1 μM; GI254023X (Selleckchem; S8660), 25 μM; TAPI-I (Selleckchem; S7434) 25 μM. Cells were pretreated with inhibitor for 30 min prior to peptide stimulation, with each stimulation occurring as a reverse time course, to ensure that all samples were subjected to exposure to the drugs for the entirety of the stimulation, totaling 4.5 h of drug exposure for all no-stimulation (0 h) and stimulated conditions (4 h).

CRISPR/Cas9 gene KO in naïve CD8 T cells

WT $CD8^+$ T cells were bead-isolated from splenocytes processed to single-cell suspensions as described above. CRISPR protocols were adapted from work previously described (31, 32). We used magnetic bead-based negative selection to enrich for $CD8^+$ T cells (>90%), which were at 2 × 10^6/ml in complete RPMI (cRPMI) supplemented with 5 ng/ml recombinant IL-7 (PeproTech: Cat. No. 217-17) for 24 h at 37 °C prior to ribonucleoprotein nucleofection, to achieve KO in naïve cells without prior stimulation. All CRISPR reagents were sourced from IDT. The crRNAs used are as follows; Mm.Cas9.ADAM10.1.AC - Alt-R CRISPR-Cas9 crRNA, 10 nmol – (/AltR1/rArG rUrUrC rArArC rCrUrA rCrGrA rArUrG rArArG rGrUrU rUrUrA rGrArG rCrUrA rUrGrC rU/AltR2/), Mm.Cas9.ADAM10.1.AD - Alt-R CRISPR-Cas9 crRNA, 10 nmol – (/AltR1/rGrG rUrUrU rCrArU rCrArA rGrArC rUrCrG rUrGrG rGrUrU rUrUrA rGrArG rCrUrA rUrGrC rU/AltR2/), Mm.Cas9.ADAM17.1.AA - Alt-R CRISPR-Cas9 crRNA, 10 nmol – (/AltR1/rCrA rUrArU rArCrC rGrGrA rArCrA rCrGrU rGrUrU rUrUrA rGrArG rCrUrA rUrGrC rU/AltR2/), Mm.Cas9.ADAM17.1.AB - Alt-R CRISPR-Cas9 crRNA, 10 nmol – (/AltR1/rCrG rUrCrC rUrGrG rCrArC rCrCrC rGrArC rCrUrC rGrUrU rUrUrA rGrArG rCrUrA rUrGrC rU/AltR2/), Mm.Cas9.PRKCQ.1.AC - Alt-R CRISPR-Cas9 crRNA, 10 nmol – (/AltR1/rArU rGrUrC rArCrC rGrUrU rUrCrU rUrCrG rArArU rGrUrU rUrUrA rGrArG rCrUrA rUrGrC rU/AltR2/), Mm.Cas9.PRKCQ.1.AD - Alt-R CRISPR-Cas9 crRNA, 10 nmol - (/AltR1/rGrC rGrUrC rArArA rGrGrU rGrCrU rGrUrC rCrCrA rGrUrU rUrUrA rGrArG rCrUrA rUrGrC rU/AltR2/), Alt-R CRISPR-Cas9 tracrRNA (Cat No. 1072532), Alt-R S.p. Cas9 Nuclease V3 (Cat No. 1081058), Alt-R CRISPR-Cas9 Negative Control crRNA #1 (Cat No. 1072544), Alt-R Cas9 Electroporation Enhancer (Cat No. 1075915). Ribonucleoprotein formation was performed at a 1:1 equimolar ratio with each tracrRNA independently, to maintain a 1:1.5 Cas9:gRNA molar ratio, which was empirically determined. We thus mixed 100 μM gRNA + 61 μM Cas9 to generate ribonucleoprotein's, which were pooled immediately prior to electroporation at 1:1 for each gene targeting pair (*i.e.*, PRKCQ.1.AD + PRKCQ.1.AC). Electroporation was performed using Lonza P3 Primary Cell 4D-Nucleofector X Kit, using pulse setting "DS 137." Following electroporation, cells were immediately placed in cRPMI (2 × 10^6 cells/ml) supplemented with 5 ng/ml rIL-7 and 20% BGS (Hyclone) to support viability and recovery. T cells were maintained in cRPMI + 5 ng/ml rIL-7 for at least five additional days following nucleofection to allow for protein turnover. The absence of prior stimulation necessitated these additional days in culture so that we could assess stimulation-dependent protein degradation, as noted in previous reports (31, 32). Cells were stimulated after day 7 in culture with 3 μg/ml plate coated anti-CD3 (clone:145-2C11; Tonbo Biosciences 50-201-4837) for the time points indicated.

Data availability

All data are contained in the manuscript and/or can be shared upon request.

Acknowledgments—This work was supported by grants from the NIH (F31CA261039 and T32CA082084 to B. M.) and (R01 GM136148 to L. P. K.). We would like to thank Grace Bowman and Edgar Cardona for their help with mouse genotyping. We would also like to thank the Unified Flow Cytometry Core.

Author contributions—B. M. M., S. C. R., H. B., L. L., U. N. U., and A. L. S.-W. investigation; B. M. M., S. C. R., and U. N. U. formal analysis; B. M. M., S. C. R., H. B., U. N. U., and L. P. K. conceptualization; B. M. M., S. C. R., and U. N. U. data curation; B. M. M., H. B., A. L. S.-W., and L. P. K. writing–review and editing; B. M. M. and

L. P. K. funding acquisition; B. M. M. writing–original draft; L. P. K. supervision.

Conflict of interest—The authors declare that they have no conflicts of interest with the contents of this article.

Abbreviations—The abbreviations used are: cRPMI, complete RPMI; DAG, diacylglycerol; HEK, human embryonic kidney; IL, interleukin; mAb, monoclonal antibody; mTrIP, murine TrIP; PI, phosphoinositide; PIK3IP1, PI3K-interacting protein; PKC, protein kinase C; PMA, phorbol 12-myristate 13-acetate; pS6, phosphorylation of the S6 ribosomal subunit; TCR, T-cell receptor.

References

1. Toker, A. (2002) Phosphoinositides and signal transduction. *Cell Mol. Life Sci.* **59**, 761–779
2. Kapeller, R., and Cantley, L. C. (1994) Phosphatidylinositol 3-kinase. *Bioessays.* **16**, 565–576
3. Anderson, R. A., Boronenkov, I. V., Doughman, S. D., Kunz, J., and Loijens, J. C. (1999) Phosphatidylinositol phosphate kinases, a multifaceted family of signaling enzymes. *J. Biol. Chem.* **274**, 9907–9910
4. Madsen, R. R., and Vanhaesebroeck, B. (2020) Cracking the context-specific PI3K signaling code. *Sci. Signal.* https://doi.org/10.1126/scisignal.aay2940
5. Okkenhaug, K., Turner, M., and Gold, M. R. (2014) PI3K signaling in B cell and T cell biology. *Front. Immunol.* **5**, 557
6. Fruman, D. A., and Bismuth, G. (2009) Fine tuning the immune response with PI3K. *Immunol. Rev.* **228**, 253–272
7. Murter, B., and Kane, L. P. (2020) Control of T lymphocyte fate decisions by PI3K signaling. *F1000Res.* https://doi.org/10.12688/f1000research.26928.1
8. Ward, S. G., and Cantrell, D. A. (2001) Phosphoinositide 3-kinases in T lymphocyte activation. *Curr. Opin. Immunol.* **13**, 332–338
9. Zambricki, E., Shigeoka, A., Kishimoto, H., Sprent, J., Burakoff, S., Carpenter, C., *et al.* (2005) Signaling T-cell survival and death by IL-2 and IL-15. *Am. J. Transpl.* **5**, 2623–2631
10. Srivastava, N., Sudan, R., and Kerr, W. G. (2013) Role of inositol polyphosphatases and their targets in T cell biology. *Front. Immunol.* **4**, 288
11. Fruman, D. A., Chiu, H., Hopkins, B. D., Bagrodia, S., Cantley, L. C., and Abraham, R. T. (2017) The PI3K pathway in human disease. *Cell* **170**, 605–635
12. Lucas, C. L., Chandra, A., Nejentsev, S., Condliffe, A. M., and Okkenhaug, K. (2016) PI3Kδ and primary immunodeficiencies. *Nat. Rev. Immunol.* **16**, 702–714
13. Preite, S., Gomez-Rodriguez, J., Cannons, J. L., and Schwartzberg, P. L. (2019) T and B-cell signaling in activated PI3K delta syndrome: from immunodeficiency to autoimmunity. *Immunol. Rev.* **291**, 154–173
14. Andreotti, A. H., Schwartzberg, P. L., Joseph, R. E., and Berg, L. J. (2010) T-cell signaling regulated by the Tec family kinase. *Itk. Cold Spring Harb. Perspect. Biol.* **2**, a002287
15. DeFrances, M. C., Debelius, D. R., Cheng, J., and Kane, L. P. (2012) Inhibition of T-cell activation by PIK3IP1. *Eur. J. Immunol.* **42**, 2754–2759
16. Uche, U. U., Piccirillo, A. R., Kataoka, S., Grebinoski, S. J., D'Cruz, L. M., and Kane, L. P. (2018) PIK3IP1/TrIP restricts activation of T cells through inhibition of PI3K/Akt. *J. Exp. Med.* **215**, 3165–3179
17. Chen, Y., Wang, J., Wang, X., Li, X., Song, J., Fang, J., *et al.* (2019) Pik3ip1 is a negative immune regulator that inhibits antitumor T-cell immunity. *Clin. Cancer Res.* **25**, 6180–6194
18. Zhu, Z., He, X., Johnson, C., Stoops, J., Eaker, A. E., Stoffer, D. S., *et al.* (2007) PI3K is negatively regulated by PIK3IP1, a novel p110 interacting protein. *Biochem. Biophys. Res. Commun.* **358**, 66–72
19. Teasley, H. E., Chang, H. J., Kim, T. H., Ku, B. J., and Jeong, J.-W. (2018) Expression of PIK3IP1 in the murine uterus during early pregnancy. *Biochem. Biophys. Res. Commun.* **495**, 2553–2558
20. Song, H. K., Kim, J., Lee, J. S., Nho, K. J., Jeong, H. C., Kim, J., *et al.* (2015) Pik3ip1 modulates cardiac hypertrophy by inhibiting PI3K pathway. *PLoS ONE* **10**, e0122251
21. Heng, T. S. P., Painter, M. W., and Immunological Genome Project Consortium (2008) The Immunological Genome Project: networks of gene expression in immune cells. *Nat. Immunol.* **9**, 1091–1094
22. Sidhom, J.-W., Theodros, D., Murter, B., Zarif, J. C., Ganguly, S., Pardoll, D. M., *et al.* (2019) ExCYT: a graphical user interface for streamlining analysis of high-dimensional cytometry data. *J. Vis. Exp.* https://doi.org/10.3791/57473
23. Boulter, J. M., Schmitz, N., Sewell, A. K., Godkin, A. J., Bachmann, M. F., and Gallimore, A. M. (2007) Potent T cell agonism mediated by a very rapid TCR/pMHC interaction. *Eur. J. Immunol.* **37**, 798–806
24. Newton, A. C. (2018) Protein kinase C: perfectly balanced. *Crit. Rev. Biochem. Mol. Biol.* **53**, 208–230
25. Anastassiadis, T., Deacon, S. W., Devarajan, K., Ma, H., and Peterson, J. R. (2011) Comprehensive assay of kinase catalytic activity reveals features of kinase inhibitor selectivity. *Nat. Biotechnol.* **29**, 1039–1045
26. Salerno, F., Paolini, N. A., Stark, R., von Lindern, M., and Wolkers, M. C. (2017) Distinct PKC-mediated posttranscriptional events set cytokine production kinetics in CD8+ T cells. *Proc. Natl. Acad. Sci. U. S. A.* **114**, 9677–9682
27. Isakov, N., and Altman, A. (2012) PKC-theta-mediated signal delivery from the TCR/CD28 surface receptors. *Front. Immunol.* **3**, 273
28. Black, R. A., and White, J. M. (1998) ADAMs: focus on the protease domain. *Curr. Opin. Cell Biol.* **10**, 654–659
29. Pfeifhofer-Obermair, C., Thuille, N., and Baier, G. (2012) Involvement of distinct PKC gene products in T cell functions. *Front. Immunol.* **3**, 220
30. Müllberg, J., Schooltink, H., Stoyan, T., Heinrich, P. C., and Rose-John, S. (1992) Protein kinase C activity is rate limiting for shedding of the interleukin-6 receptor. *Biochem. Biophys. Res. Commun.* **189**, 794–800
31. Seki, A., and Rutz, S. (2018) Optimized RNP transfection for highly efficient CRISPR/Cas9-mediated gene knockout in primary T cells. *J. Exp. Med.* **215**, 985–997
32. Oh, S. A., Seki, A., and Rutz, S. (2019) Ribonucleoprotein transfection for CRISPR/Cas9-Mediated gene knockout in primary T cells. *Curr. Protoc. Immunol.* **124**, e69
33. Herzog, C., Haun, R. S., Ludwig, A., Shah, S. V., and Kaushal, G. P. (2014) ADAM10 is the major sheddase responsible for the release of membrane-associated meprin A. *J. Biol. Chem.* **289**, 13308–13322
34. Maretzky, T., Reiss, K., Ludwig, A., Buchholz, J., Scholz, F., Proksch, E., *et al.* (2005) ADAM10 mediates E-cadherin shedding and regulates epithelial cell-cell adhesion, migration, and beta-catenin translocation. *Proc. Natl. Acad. Sci. U. S. A.* **102**, 9182–9187
35. Lorenzen, I., Lokau, J., Korpys, Y., Oldefest, M., Flynn, C. M., Künzel, U., *et al.* (2016) Control of ADAM17 activity by regulation of its cellular localisation. *Sci. Rep.* **6**, 35067
36. Senior, A. W., Evans, R., Jumper, J., Kirkpatrick, J., Sifre, L., Green, T., *et al.* (2020) Improved protein structure prediction using potentials from deep learning. *Nature* **577**, 706–710
37. Heo, L., and Feig, M. (2020) High-accuracy protein structures by combining machine-learning with physics-based refinement. *Proteins* **88**, 637–642
38. Song, J., Wang, Y., Li, F., Akutsu, T., Rawlings, N. D., Webb, G. I., *et al.* (2019) iProt-Sub: a comprehensive package for accurately mapping and predicting protease-specific substrates and cleavage sites. *Brief. Bioinformatics* **20**, 638–658
39. Scheller, J., Chalaris, A., Garbers, C., and Rose-John, S. (2011) ADAM17: a molecular switch to control inflammation and tissue regeneration. *Trends Immunol.* **32**, 380–387
40. Zunke, F., and Rose-John, S. (2017) The shedding protease ADAM17: physiology and pathophysiology. *Biochim. Biophys. Acta Mol. Cell Res.* **1864**, 2059–2070
41. Mishra, H. K., Ma, J., and Walcheck, B. (2017) Ectodomain shedding by ADAM17: its role in neutrophil recruitment and the impairment of this process during sepsis. *Front. Cell. Infect. Microbiol.* **7**, 138
42. Steinberg, S. F. (2008) Structural basis of protein kinase C isoform function. *Physiol. Rev.* **88**, 1341–1378

43. Padmanabhan, K., Wu, T. P., Ravichandran, K. G., and Tulinsky, A. (1994) Kringle-kringle interactions in multimer kringle structures. *Protein Sci.* **3**, 898–910
44. Castellino, F. J., and McCance, S. G. (1997) The kringle domains of human plasminogen. *Ciba Found. Symp.* **212**, 46–60. discussion 60
45. Cibrián, D., and Sánchez-Madrid, F. (2017) CD69: from activation marker to metabolic gatekeeper. *Eur. J. Immunol.* **47**, 946–953
46. Wang, X., Hills, L. B., and Huang, Y. H. (2015) Lipid and protein Co-regulation of PI3K effectors Akt and Itk in lymphocytes. *Front. Immunol.* **6**, 117
47. Rosse, C., Linch, M., Kermorgant, S., Cameron, A. J. M., Boeckeler, K., and Parker, P. J. (2010) PKC and the control of localized signal dynamics. *Nat. Rev. Mol. Cell Biol.* **11**, 103–112
48. Altman, A., and Villalba, M. (2002) Protein kinase C-theta (PKC theta): a key enzyme in T cell life and death. *J. Biochem.* **132**, 841–846
49. Baier, G., Telford, D., Giampa, L., Coggeshall, K. M., Baier-Bitterlich, G., Isakov, N., *et al.* (1993) Molecular cloning and characterization of PKC theta, a novel member of the protein kinase C (PKC) gene family expressed predominantly in hematopoietic cells. *J. Biol. Chem.* **268**, 4997–5004
50. Pfeifhofer, C., Kofler, K., Gruber, T., Tabrizi, N. G., Lutz, C., Maly, K., *et al.* (2003) Protein kinase C theta affects Ca2+ mobilization and NFAT cell activation in primary mouse T cells. *J. Exp. Med.* **197**, 1525–1535
51. Saftig, P., and Reiss, K. (2011) The "A Disintegrin and Metalloproteases" ADAM10 and ADAM17: novel drug targets with therapeutic potential? *Eur. J. Cell Biol.* **90**, 527–535
52. Möller-Hackbarth, K., Dewitz, C., Schweigert, O., Trad, A., Garbers, C., Rose-John, S., *et al.* (2013) A disintegrin and metalloprotease (ADAM) 10 and ADAM17 are major sheddases of T cell immunoglobulin and mucin domain 3 (Tim-3). *J. Biol. Chem.* **288**, 34529–34544
53. Le Gall, S. M., Bobé, P., Reiss, K., Horiuchi, K., Niu, X.-D., Lundell, D., *et al.* (2009) ADAMs 10 and 17 represent differentially regulated components of a general shedding machinery for membrane proteins such as transforming growth factor alpha, L-selectin, and tumor necrosis factor alpha. *Mol. Biol. Cell.* **20**, 1785–1794
54. Andrews, L. P., Somasundaram, A., Moskovitz, J. M., Szymczak-Workman, A. L., Liu, C., Cillo, A. R., *et al.* (2020) Resistance to PD1 blockade in the absence of metalloprotease-mediated LAG3 shedding. *Sci. Immunol.* https://doi.org/10.1126/sciimmunol.abc2728